Bulk and Single Crystal Growth Progress of FBS

Subjects: Physics, Applied | Physics, Condensed Matter

Contributor: Shiv J. Singh

The new iron-based superconductor (FBS) has generated enormous interest in this direction, and many research activities are currently going on with various kinds of FBS. FBS was discovered in 2008 through F doped LaFeAsO, which crystallizes with a tetragonal layered ZrCuSiAs structure, and after that, many compounds have been discovered, most of which display superconductivity through suitable doping. FBS became the second high-Tc-superconducting family after cuprate superconductors and has been the subject of extensive research into their physical nature and application potential.

high superconductors | transition temperature | synthesis and crystal growth | polycrystalline and single crystal | iron-based superconductors

1. Family 1111

The 1111-type bulk superconductors have been widely studied to achieve a record T_c by various doping methods, external pressure, or synthesizing techniques [1][2][3]. Following the first report of $LaFeAsO_{1-x}F_x$ with T_c around 26 K [4], a high-pressure synthesis method quickly observed an increase in T_c up to 55 K in $SmFeAsO_{1-x}F_x$ and $SmFeAsO_{1-\delta}$ [5]. Usually, the electron doping in 1111 such as F doping in the LaO layer of La1111 [6], Th doping in the LaO layer of La1111 [7], and even H doping in the LaO layer [8] results in almost similar T_c, whereas the chemical doping in superconducting FeAs layers [9][10][11][12][13] generally leads to a lowering of T_c such as Co, Mn, Ni, P doped FeAs layer [11][12][13] as mentioned in **Table 1**. The effects of applied external pressure on the transition temperature have also been studied for this 1111 family [14]. Interestingly, the applied pressure improved the superconducting transition T_c from 26 K to 43 K for $LaFeAsO_{0.89}F_{0.11}$ (La1111), nevertheless, it reduced the T_c for $CeFeAsO_{0.88}F_{0.12}$ (Ce1111) and $REFeAsO_{0.85}$ (RE1111) (*RE* = Sm and Nd) [14]. Moreover, superconductivity at 57.8 K was found in $SmFeAsO_{1-x}F_x$ film grown by molecular beam epitaxy [15]. Recently, several groups found that low-temperature sintering and slow-cooling techniques could introduce high F-doping levels with T_c enhanced up to 58 K in $SmFeAsO_{1-x}F_x$ [1][2]. Furthermore, the Th and F co-doped $Sm_{1-x}Th_xFeAsO_{1-y}F_y$ samples synthesized by the solid-state reaction can effectively enhance superconductivity, resulting in a maximum T_c of 58.6 K [3].

Table 1. A list of polycrystalline samples reported for the 1111 (*RE*FeAsO) and 1144 ($AEAFe_4As_4$) families, along with their synthesis conditions and superconducting properties. T^{syn} is used for the synthesis temperature and heating time. The Solid-State Reaction (SSR) method at high pressure and ambient pressure is represented by the

high-pressure synthesis technique (HPST) and the conventional synthesis process at ambient pressure (CSP-AP), respectively.

Sample	Synthesis Method and Conditions	Superconducting Properties
LaFeAs(O,F)	CSP-AP, T^{syn} = 1180 °C, 48 h	T^{max}_c = 28.5 K, $H_{c2}(0)$ = 105 T [6]
(La,K)FeAs(O,F)	CSP-AP, T^{syn} = 1180 °C, 48 h	T^{max}_c = 26.5 K, $H_{c2}(0)$ = 122 T [6]
$LaFeAsO_{1-y}$	HPST, T^{syn} = 1100–1200 °C, 2 h	T^{max}_c = 28 K [16]
(La,Sr)FeAs	CSP-AP, T^{syn} = 1150 °C, 40 h	T^{max}_c = 26 K [17]
(La,Y)FeAs(O,F)	CSP-AP, T^{syn} = 1250 °C, 25 h	T^{max}_c = 40.2 K, $H_{c2}(0)$ = 60.5 T [18][19]
$(La,Y)FeAsO_{0.6}$	HPST, T^{syn} = 1150 °C, 2 h	T^{max}_c = 43.1 K [20]
LaFe(As,Sb)(O,F)	CSP-AP, T^{syn} = 1150 °C, 48 h	T^{max}_c = 30.1 K, $H_{c2}(0)$ = 73 T [21]
La(Fe,Co)AsO	CSP-AP, T^{syn} = 1220 °C, 12 h	T^{max}_c = ~14.3 K [22]
(La,Th)FeAsO	CSP-AP, T^{syn} = 1180 °C, 48 h	T^{max}_c = 30.3 K, $H_{c2}(0)$ = 47 T [7]
LaFe(As,P)O	CSP-AP, T^{syn} = 1100 °C, 40 h	T^{max}_c = 10 K, $H_{c2}(0)$ = 27 T [23]
$LaFe_{0.95}Co_{0.05}AsO_{0.89}F_{0.11}$	CSP-AP, T^{syn} = 1150 °C, 48 h	T^{max}_c = ~15 K [24]
$LaFe_{0.99}Co_{0.01}AsO_{0.89}F_{0.11}$	CSP-AP, T^{syn} = 1150 °C, 48 h	T^{max}_c = ~10 K [24]
$LaFeAsO_{0.6}H_{0.6}$	HPST, T^{syn} = 1100 °C, 2 h	T^{max}_c = ~38.3 K [25]
CeFeAs(O,F)	CSP-AP, T^{syn} = 1180 °C, 48 h	T^{max}_c = 42.5 K, $H_{c2}(0)$ = 94 T [26]
(Ce,Y)FeAs(O,F)	CSP-AP, T^{syn} = 1100 °C, 30 h	T^{max}_c = 48.6 K, $H_{c2}(0)$ = 90 T [27]
CeFe(As,P)O	CSP-AP, T^{syn} = 1175 °C, 50 h	T^{max}_c ~4 K [28][29]
$CeFe(As,P)O_{0.95}F_{0.05}$	CSP-AP, T^{syn} = 1175 °C, 50 h	T^{max}_c = 21.3 K [30]
Ce(Fe,Co)As(O,F)	CSP-AP, T^{syn} = 1150 °C, 48 h	T^{max}_c = 23.4 K, $H_{c2}(0)$ = 25.3 T [31]
Ce(Fe,Co)AsO	CSP-AP, T^{syn} = 1180 °C, 48 h	T^{max}_c = 11.31 K, $H_{c2}(0)$ = 45.2 T [10]
Ce(Fe,Ni)AsO	CSP-AP, T^{syn} = 1150 °C, 48 h	No T_c [12]
Ce(Fe,Zn)AsO	CSP-AP, T^{syn} = 1150 °C, 48 h	No T_c [12]
CeFe(As,Sb)(O,F)	CSP-AP, T^{syn} = 1180 °C, 48 h	T^{max}_c = 43.17 K, $H_{c2}(0)$ = 137 T [32]

Sample	Synthesis Method and Conditions	Superconducting Properties
$CeFeAsO_{0.6}H_{0.6}$	HPST, T^{syn} = 1100 °C, 2 h	T^{max}_c = ~47.9 K [25]
PrFeAs(O,F)	CSP-AP, T^{syn} = 1150 °C, 24 h	T^{max}_c = 50 K [33]
Pr(Fe,Co)AsO	CSP-AP, T^{syn} = 1100 °C, 48 h	T^{max}_c = 16 K, $H_{c2}(0)$ = 50.2 T [9]
(Pr,Sr)(Fe,Co)AsO	CSP-AP, T^{syn} = 1160 °C, 40 h	T^{max}_c= 16 K [34]
$PrFeAsO_{0.6}H_{0.6}$	HPST, T^{syn} = 1100 °C, 2 h	T^{max}_c = ~51.9 K [25]
$NdFeAsO_{1-y}$	HPST, T^{syn} = 1100–1200 °C, 2 h	T^{max}_c = 54 K [16][35]
NdFeAs(O,F)	CSP-AP, T^{syn} = 1350 °C, 15 h	T^{max}_c = 55 K [36][37]
(Nd,Gd)FeAs(O,F)	CSP-AP, T^{syn} = 1350 °C, 15 h	T^{max}_c = 55.1 K, J_c(5K) = 3.4 × 10^3 A/cm^2 [38]
Nd(Fe,Rh)AsO	CSP-AP, T^{syn} = 1150 °C, 48 h	T^{max}_c = 18 K, $H_{c2}(0)$ = 100 T [39]
$NdFe_{0.85}Ru_{0.15}AsO_{0.89}F_{0.11}$	CSP-AP, T^{syn} = 1150 °C, 48 h	T^{max}_c = 34 K [40]
$NdFe_{0.9}Co_{0.1}AsO_{0.89}F_{0.11}$	CSP-AP, T^{syn} = 1150 °C, 48 h	T^{max}_c = ~18 K [24]
$NdFe_{0.98}Mn_{0.02}AsO_{0.89}F_{0.11}$	CSP-AP, T^{syn} = 1150 °C, 48 h	T^{max}_c = ~27 K [24]
$Nd_{0.99}Ca_{0.01}FeAsO_{0.8}F_{0.2}$	CSP-AP, T^{syn} = 1150 °C, 20 h	T^{max}_c = ~48 K [41]
Nd(Fe,Co)AsO	CSP-AP, T^{syn} = 1150 °C, 48 h	T^{max}_c = ~16.5 K, $H_{c2}(0)$ = 26 T [42]
SmFeAs(O,F)	CSP-AP, T^{syn} = 900 °C, 45 h	T^{max}_c = 57.8 K, $H_{c2}(0)$ = 315 T [1]
SmFeAs(O,F)	CSP-AP, T^{syn} = 980 °C, 40 h	T^{max}_c = 58.1 K [2]
(Sm,Th)FeAs(O,F)	CSP-AP, T^{syn} = 1150 °C, 30 h	T^{max}_c = 58.6 K [3]
Sm(Fe,Co)AsO	CSP-AP, T^{syn} = 1180 °C, 45 h	T^{max}_c = 15.2 K [43]
(Sm,Sc)FeAs(O,F)	CSP-AP, T^{syn} = 950 °C, 2 h	T^{max}_c = 53.5 K, $H_{c2}(0)$ = 298 T [44]
(Sm,Th)FeAsO	CSP-AP, T^{syn} = 1150 °C, 30 h	T^{max}_c = 45 K [3]
$Sm_{0.9}Y_{0.1}FeAsO_{0.8}F_{0.2}$	CSP-AP, T^{syn} = 1300 °C, 40 h	T^{max}_c = 43 K [45]
Sm(Fe,Ir)AsO	CSP-AP, T^{syn} = 1150 °C, 48 h	T^{max}_c = 16 K [46]
$SmFe_{0.97}Mn_{0.03}As(O,F)$	CSP-AP, T^{syn} = 900 °C, 45 h	T^{max}_c = 30 K, $H_{c2}(0)$ = 205 T [11]
$SmFe_{0.94}Mn_{0.06}AsO_{0.88}F_{0.12}$	CSP-AP, T^{syn} = 900 °C, 45 h	T^{max}_c = 16.5 K, $H_{c2}(0)$ = 43 T [11]

Sample	Synthesis Method and Conditions	Superconducting Properties
$SmFe_{0.94}Ni_{0.06}AsO_{0.88}F_{0.12}$	CSP-AP, T^{syn} = 900 °C, 45 h	T^{max}_c = 18 K, $H_{c2}(0)$ = 47 T [11]
$SmFe_{0.94}Ni_{0.03}AsO_{0.88}F_{0.12}$	CSP-AP, T^{syn} = 900 °C, 45 h	T^{max}_c = 33 K, $H_{c2}(0)$ = 200 T [11]
$SmFeAs_{0.95}P_{0.05}O_{0.88}F_{0.12}$	CSP-AP, T^{syn} = 900 °C, 45 h	T^{max}_c = 40 K, $H_{c2}(0)$ = 292 T [13]
$SmFeAs_{0.8}P_{0.2}O_{0.88}F_{0.12}$	CSP-AP, T^{syn} = 900 °C, 45 h	T^{max}_c = 20 K, $H_{c2}(0)$ = 31 T [13]
$SmFeAsO_{1-x}$	HPST, T^{syn} = 1300 °C, 2 h	T^{max}_c = 57 K, $H_{c2}(0)$ = 60 T [5]
(Gd,Th)FeAsO	HPST, T^{syn} = 1300 °C, 2 h	T^{max}_c = 56 K [47]
$GdFeAsO_{1-x}$	HPST, T^{syn} = 1350 °C, 2 h	T^{max}_c = 56 K [48][49]
GdFeAs(O,F)	HPST, T^{syn} = 1350 °C, 2 h	T^{max}_c = 51.2 K, $H_{c2}(0)$ = 20 T [48]
GdFeAs(O,F)	CSP-AP, T^{syn} = 1150 °C, 48 h	T^{max}_c = 36.6 K [50]
Gd(Fe,Ir)FeAsO	CSP-AP, T^{syn} = 1200 °C, 72 h	T^{max}_c = 18.9 K, $H_{c2}(0)$ = 24 T [51]
$Sr_{1-x}Sm_xFeAsF$	CSP-AP, T^{syn} = 1000 °C, 10 h	T^{max}_c = 56 K [52]
$CaFe_{1-x}Co_xAsF$	CSP-AP, T^{syn} = 1000 °C, 10 h	T^{max}_c = 22 K [53]
$CaKFe_4As_4$	CSP-AP, T^{syn} = 860–920 °C, 2–6 h	T^{max}_c = 33.1 K [54]
$CaRbFe_4As_4$	CSP-AP, T^{syn} = 860–920 °C, 2–6 h	T^{max}_c = 35 K [54]
$CaCsFe_4As_4$	CSP-AP, T^{syn} = 860–920 °C, 2–6 h	T^{max}_c = 31.6 K [54]
$SrRbFe_4As_4$	CSP-AP, T^{syn} = 860–920 °C, 2–6 h	T^{max}_c = 35.1 K [54]
$SrCsFe_4As_4$	CSP-AP, T^{syn} = 860–920 °C, 2–6 h	T^{max}_c = 36.8 K [54]
$CaKFe_4As_4$	CSP-AP, T^{syn} = 955 °C, 6 h	T^{max}_c = 34.2 K, $H_{c2}(0)$ = 138 T [55]

generally
phase at
the SSR
ed to as
echniques
performed
etal tube,
oing at O-
Table 1).

Generally, the highest T_c is obtained by F doping, and a lot of work has been done with F-doping, but the control of this dopant according to the composition is not a very easy task through CSP-AP. In contrast, since the 1111-type compounds contain at least four components, in the case of dopants, more than five elements are included, and precisely controlling their composition is very difficult. During the initial synthesis process, even if starting materials are mixed at the correct composition ratio, the prepared substance contains a spurious phase whose composition differs from the nominal one for many polycrystalline materials. For example, in the case of Sm1111, the impurity phases of SmOF, SmAs, and/or Sm_2O_3 are formed, and their concentrations generally increase as the dopant concentration increases in $SmFeAsO_{1-x}F_x$ [1][56]. It is a very common situation for other members of the 1111 family, especially those containing rare earth elements. The impurity phase of *RE*FO is stable, and it is not so easy to eliminate. From quantitative analysis, Malavasi et al. [57] demonstrated the difference in composition between nominal and prepared $NdFeAsO_{12x}F_x$ and noted that the measured F-content in a specimen with the nominal

composition of $NdFeAsO_{0.78}F_{0.22}$ is 0.188. The relationship between the nominal F content and the real one is determined through electron probe microanalysis [57].

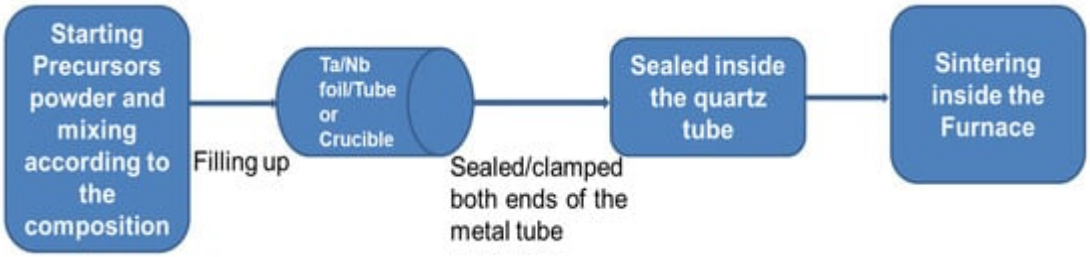

Figure 1. A general block diagram of the Solid-State Reaction (SSR) method for FBS.

To overcome these problems, a high-pressure solid-state reaction method has been used for the 1111 family. The high-pressure synthesis technique (HPST) has been utilized for preparing a series of oxygen-deficient *RE*FeAsO (*RE* = La and Nd) polycrystalline samples [16][35]. The introduction of oxygen vacancies causes a decrease in lattice parameters, and superconductivity appears when the *a*- and *c*-axis lattice parameters shrink by 0.1% when compared to undoped compounds (*RE*FeAsO). When *RE* = La is replaced with *RE* = Nd in *RE*1111, the *a*-lattice parameter is decreased by 0.2%, and the maximum T_c is increased from 28 K to 54 K [16][35]. Further O-deficiency in La1111 eventually results in the reduction of T_c [16]. On the other hand, in the case of Nd1111, the maximum T_c value is robust against the introduction of O-deficiency, suggesting that the superconducting region is much narrower for La1111 than for Nd1111 [16][35]. Similarly, hydrogen doping of Sm1111 and Ce1111 is not possible via CSP-AP, but HPST (2 GPa and 1200 °C) can produce a series of H-doped 1111 [8][16]. These studies have depicted the unique behavior of two superconducting domes in the phase diagram and highlight the new findings of FBS that generate the new physics and new doping effects in 1111 by HPST, whereas single dome behavior is observed in the phase diagram of F-doped 1111 through CSP-AP. In the case of H-doped 1111, the first dome is similar to F-doped La1111 (through CSP-AP), but the range of the second dome is much wider than that reported in the F-substituted case for the other rare earth (*RE*) systems [8]. Kametani et al. [58] have reported polycrystalline $SmFeAsO_{0.85}$ and $NdFeAsO_{0.94}F_{0.06}$ bulk samples synthesized by solid-state reaction under high pressure. These samples are better than the CSP-AP samples, but impurity phases and cracks were found during the microstructural analysis. Furthermore, two distinct scales of current, i.e., intergrain and intragrain current, are observed in the reported polycrystalline samples, which suggests an electromagnetic granular nature of 1111 [59][55][60]. It implies that a locally circulating intragrain supercurrent and others due to intergrain pinning exist in the bulk sample. Microstructural analysis shows the presence of macroscopic inhomogeneity, and cracks and wetting amorphous phases at grain boundaries [58]. Because of these extrinsic factors, the intergrain J_c has a very low value for these samples [59][55][60]. **Figure 2** summarizes the 1111 family's transition temperature T_c dependence on the reported intergrain J_c with various FBS. Many groups have optimized the synthesis parameters during solid-state reaction methods such as low-temperature synthesis and have improved the sample quality [1][2]. However, the obtained samples always have problems with grain connectivity and impurity phases. For these reasons, the obtained intergrain J_c value of the 1111 family is very small, as shown in **Figure 2**, for the requirements of practical applications. To improve the grain connectivity and critical current properties, various techniques such as metal

additions (Sn, Pb, Ag, Zn, In), cold or hot pressing, and hot isostatic pressing could be useful during the synthesis process of the polycrystalline samples, which generally improve the microstructure as reported for FBS wires/tapes fabrication [61]. For example, Singh et al. have studied the effect of Sn addition in Sm1111, where Sn additions reduced the impurity phases in $SmFeAsO_{0.8}F_{0.2}$ [61][62], increasing clean and well-connected grain boundaries. Remanent magnetization measurements revealed that Sn addition improved the intergrain J_c at 5 K from 1×10^2 to 1.1×10^4 A cm^{-2} for $SmFeAsO_{0.8}F_{0.2}$ and from 4×10^3 to 9.7×10^3 A cm^{-2} for $SmFeAsO_{0.88}F_{0.12}$ [62], as shown in **Figure 3**. This enhancement of the intergrain J_c might be attributable to the strong intergrain coupling due to the improved grain connectivity by the Sn additions. However, these obtained values are still much lower than the practical level, which suggests further improvement of grain size and grain connections is required by reducing the extrinsic factors [61][58][60][62]. Hence, we need more research in this direction through advanced techniques.

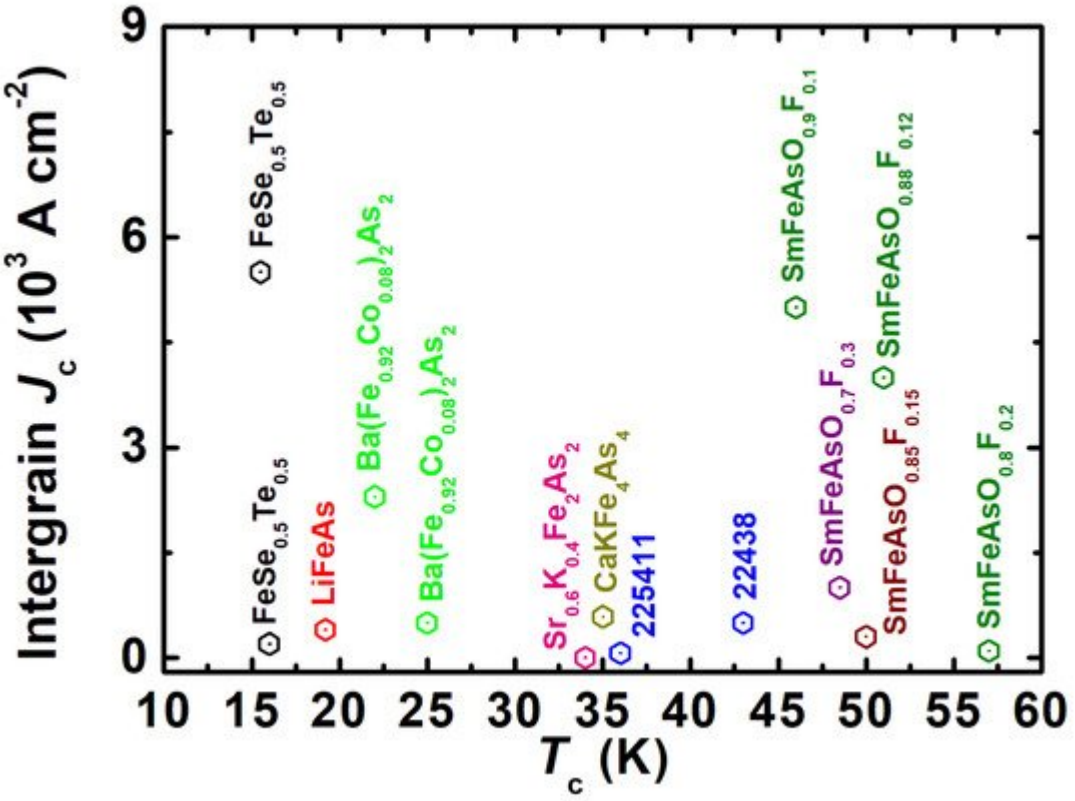

Figure 2. The transition temperature (T_c) dependence of the intergrain J_c calculated from the remanent magnetization measurements for different FBS families together with that of the 1111 and 1144 families. All the mentioned samples are prepared by the conventional synthesis process at ambient pressure (CSP-AP). The data were gathered from the references [63][64][59][55][60][65][66][67][68].

Single crystals: Many groups have reported the single crystal growth of this family [69][70][71][72][73][74][75][76][77] using different growth parameters. However, it is not an easy task to obtain high-quality and suitable-sized 1111 crystals. Despite many efforts in the last 12 years, the grown crystals of 1111 are still limited in dimensions [69][77], struggling to keep the nominal composition as the actual composition and to reduce secondary phases or impurities. Due to these problems, the existing results are debatable, and at the moment, a consensus has not

been reached yet, similar to other FBS families. For example, a lot of studies have been done on 122 materials with various doping elements (K for Ba, Co for Fe, and P for As) and with different doping concentrations [78][79][80][81]. The reported J_c values determined by magnetic hysteresis loop (MHL) measurements are controversial even for the same types of doped crystals. For example, the doping dependence of J_c follows the doping dependence of T_c for Ba(Fe, Co)$_2$As$_2$, whereas other reports show that J_c does not follow T_c and is highest in the underdoped region for Ba(Fe, Co)$_2$As$_2$ and (Ba, K)Fe$_2$As$_2$ where different pinning sources are also proposed [82][80][83][84]. Extrinsic factors, rather than doping concentration, determine J_c in BaFe$_2$(As,P)$_2$ [80][81]. Due to these issues, there are many unresolved features concerning their superconducting properties. Mostly, the following two methods are used to grow the single crystals of the 1111 family:

(a) Flux methods: Generally, the melt-solidification process cannot work for these compounds due to the presence of many elements that tend to form incongruent melting compounds. Thus, the solution-growth process is needed, and the final growth temperature must be lower than the decomposition temperature of the final compound. In this direction, one of the useful methods is the “flux method”. The flux growth method at ambient pressure is used significantly for this family because this method generally helps to start the reaction much lower than that used for solid-state reaction methods. A general block diagram for the self-flux method is shown in **Figure 3**. The details of the reported 1111 crystals are mentioned in **Table 2** with their growth conditions and superconducting properties. FM-AP is used for the Flux method at ambient pressure. Quebe et al. [70] have reported the crystal growth of the parent compound *RE*FeAsO through NaCl/KCl flux. Single crystals of PrFeAsO and NdFeAsO with a size of 70–100 µm have been grown from alkali-metal chloride flux. Fang et al. [72] have used this method to grow NdFeAs and NdFeAsO$_{0.7}$F$_{0.3}$ at ambient pressure. Jesche et al. [73] have grown larger single crystals of CeFeAsO using a Sn-flux technique. Yan et al. [85] used NaAs to grow large single crystals of LaFeAsO, LaFeAs(O, F), and LaFe$_{0.92}$Co$_{0.08}$AsO at ambient pressure, and Jesche et al. [73] used Sn as a flux to grow CeFeAsO at ambient pressure. Nitsche et al. [74] have grown the single crystals of *RE*FeAsO (*RE* = La, Ce, Pr, Nd, Sm, Gd, and Tb) using NaI/KI as flux and obtained crystals with a size of up to 300 µm. The first attempts to grow single crystals following previous studies on *RETM*$_x$As$_2$ (*TM* = transition metal) [75] were conducted with rare-earth metal oxide (*RE*$_2$O$_3$), arsenic, and iron as starting materials, and alkali-metal chlorides as flux. As observed before [69], *RE*OCl hindered the formation of phase-pure samples and single crystals of the target compounds. When using sodium or potassium iodide, the less stable oxide iodides (*RE*OI) are not formed. As an oxygen source, the exchange of rare-earth metal oxide by iron (III)-oxide or better by iron (II)-oxide improved single-crystal growth. However, the synthesis of *RE*FeAsO with rare-earth metals heavier than terbium failed to apply the NaI/KI flux method [70][74]. Unfortunately, according to published papers [86][69], 1111 single crystals via flux growth are difficult to obtain [70][74]. This is because these are oxides facing the hurdle of the low solubility of oxygen in liquid metals at 1100 °C excluding their growth from “classical” metal fluxes and their self-flux variants [87]. However, the ambient pressure reaction process usually limits the synthesis temperature [87][88][89][90][91][92] and takes a very long time to grow even a tiny crystal size. This process creates chemical inhomogeneity due to the presence of lighter elements and the high vapor pressure of arsenic.

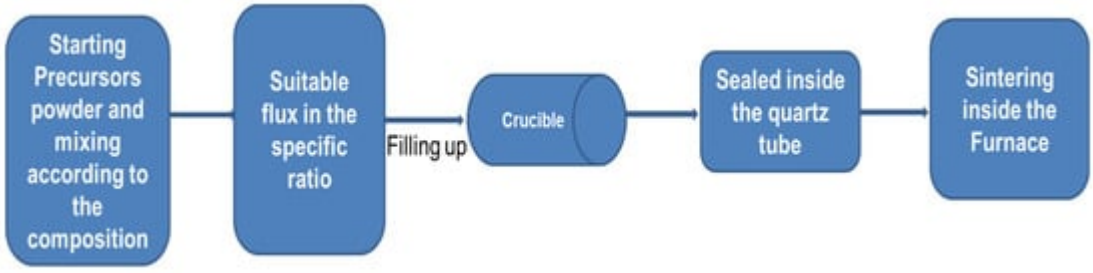

Figure 3. A general block diagram of the flux method.

Table 2. List of single crystals reported for the 1111 (*RE*FeAsO) and 1144 ($AEAFe_4As_4$) families, including growth conditions and superconducting properties. T^{syn} is used for the synthesis temperature and heating time. FM-AP and FM-HP represent Flux method at ambient pressure and the Flux method at high pressure, respectively. SSCG-AP and SSCG-HP refer to the Solid-State Crystal Growth method at ambient pressure and high pressure, respectively.

Sample	Synthesis Method and Conditions	Superconducting Properties
SmFeAs(O,F)	FM-HP, Flux: NCl/KCl, T^{syn} = 1350–1450 °C, 4–85 h	T^{max}_c = 53 K, $H_{c2}(0)$ = ~100 T, J_c(15 K,7 T) = 2 × 10^5 A/cm^2 [69]
REFeAsO	FM-AP, Flux: NaCl/KCl, T^{syn} = 800 °C, 2 weeks	No T_c [70]
$NdFeAsO_{0.9}F_{0.1}$	SSCG-HP, No Flux, T^{syn} = 1350–1400 °C, 8 h	T^{max}_c = 45 K [93][71]
$LaFeAsO_{0.9}F_{0.1}$	SSCG-HP, No Flux, T^{syn} = 1350–1400 °C, 8 h	T^{max}_c = 14 K [71]
$NdFeAsO_{0.7}F_{0.3}$	FM-AP, Flux: NCl, T^{syn} = 1050 °C, 2 weeks	T^{max}_c = 49 K, $H_{c2}(0)$ = 49 T [72]
CeFeAsO	FM-AP, Flux: Sn, T^{syn} = 1500 °C, 1 h	No T_c [73]
$CeFeAs_{0.7}P_{0.3}O$	FM-AP, Flux: Sn, T^{syn} = 1500 °C, 1 h	No T_c [73][92]
SmFeAs(O,F)	FM-AP, Flux: CsCl, T^{syn} = 950 °C, 5 h	T^{max}_c = 57.5 K, $H_{c2}(0)$ = ~330 T [56]
$PrFeAsO_{1-y}$	FM-HP, No Flux/Flux:As/FeAs/PrFeAs(O,F), T^{syn} = 1300–1400 °C, 2 h	T^{max}_c = 44 K [88]
*RE*FeAsO	FM-AP, Flux: NaI/KI, T^{syn} = 1050 °C, 6–7 days	No T_c [74]
$LaFeAsO_{0.91}F_{0.09}$	FM-AP, Flux: NaAs, T^{syn} = 1150 °C, 24 h	T_c = 11 K [85]
$LaFe_{0.98}Co_{0.02}AsO$	FM-AP, Flux: NaAs, T^{syn} = 1150 °C, 24 h	T_c = ~8 K [85]
(La/Nd)FeAsO	FM-AP, Flux: NaAs, T^{syn} = 1100 °C, 12 h	No T_c [89]
LaFeAsO	SSCG-AP, T^{syn} = 1080 °C, 200 h	No T_c [90]

Sample	Synthesis Method and Conditions	Superconducting Properties
$CaFe_{0.882}Co_{0.118}AsF$	FM-AP, Flux: CaAs, T^{syn} = 1230 °C, 20 h	T_c = 22 K [89]
Sm(Fe,Co)AsO	FM-HP, Flux: NaAs/KAs, T^{syn} = 1350–1450 °C, 4–85 h	T_c = 16.4 K, $H_{c2}(0)$ = 100 T, $J_c(2K,0T) = 1 \times 10^5$ A/cm^2 [77]
PrFeAs(O,F)	FM-HP, Flux: NaAs/KAs, T^{syn} = 1350–1450 °C, 4–85 h	T_c = 30 K, $J_c(5K,0T) = 1 \times 10^5$ A/cm^2 [77]
$PrFeAsO_{0.80-x}F_x$	FM-HP, Flux: NaCl/KCl, T^{syn} = 1350–1450 °C, 4–85 h	T_c = 38.3 K [69]
$NdFeAsO_{0.89-x}F_x$	FM-HP, Flux: NaCl/KCl, T^{syn} = 1350–1450 °C, 4–85 h	T_c = 46.3 K [69]
$GdFeAsO_{0.76-x}F_x$	FM-HP, Flux: NaCl/KCl, T^{syn} = 1350–1450 °C, 4–85 h	T_c = 22.7 K [69]
NdFeAs(O,F)	FM-HP, Flux: NaAs/KAs, T^{syn} = 1350–1450 °C, 4–85 h	T_c = 38.5 K [77]
SmFeAs(O,H)	FM-HP, Flux: Na_3As/3NaH+As/Na_3As+3NaH+As, T^{syn} = 1200 °C, 4–85 h	T_c = 43.0 K [86]
$CaKFe_4As_4$	FM-AP, Flux: FeAs, T^{syn} = 1180 °C, 5 h	T_c = 35.0 K, $H_{c2}(0)$ = ~100 T, $J_c(2K,0T)$ = ~10^7–10^8 A/cm^2 [94][95]
$CaK(Fe_{1-x}Ni_x)_4As_4$	FM-AP, Flux: FeAs, T^{syn} = 1180 °C, 5 h	T_c = 9–30 K [96]
$CaK(Fe_{1-x}Co_x)_4As_4$	FM-AP, Flux: FeAs, T^{syn} = 1180 °C, 5 h	T_c = 2–29 K [96]
$CaRbFe_4As_4$	FM-AP, Flux: FeAs, T^{syn} = 1180 °C, 2 h	T_c = 35 K [97]
$EuRbFe_4As_4$	FM-AP, Flux: FeAs, T^{syn} = 1250 °C, 24 h [69][93][16][88]	T_c = 35 K, $H_{c2}(0)$ = ~135 T [98]
$EuRbFe_4As_4$	FM-AP, Flux: RbAs, T_{syn} = 920 °C, 12 h	T_c = 37 K [99][100]

ction rate
sure. This high-pressure method enables the high-temperature reaction by reducing the vaporization of lighter elements and also reducing the inhomogeneity of the samples, which speeds up the reaction process. There are only a few reports of 1111 crystal growth by using high-pressure techniques (FM-HP), as mentioned in **Table 2**, which have resulted in the growth of slightly large and homogeneous crystals. Ishikado et al. [88] have reported the single crystal growth of $PrFeAsO_{1-y}$ in BN crucibles under a pressure of about 2 GPa at 1300–1400 °C for 2 h, and the obtained crystals were around 500 µm. Karpensiki et al. [69] adopted the high-pressure crystal-growth method and produced the *RE*1111 crystals with a size of 300 µm. They carried out a systematic investigation of the parameters controlling the growth of *RE*1111 crystals, including the thermodynamic variables, reagent composition, and kinetic factors such as reaction time and cooling rate. The high-pressure flux method using Na-As and KAs as a flux provided the slightly larger-sized 1111 crystals (up to ~1 mm) which were separated from the flux before its characterization [69]. In comparison with NaCl/KCl flux growth, these fluxes are at least three times more efficient in obtaining large-sized crystals [69]. There are reports that NaAs works as a flux, enabling the uptake of oxygen via the intermediate formation of $NaAsO_2$ yielding small crystals, and sometimes intergrowth with a 122 phase has

also been reported [85][87][101]. By applying pressure, SmFeAsO single crystals of up to 150 μm have been obtained. Using high pressure and arsenic as flux, Ishikado et al. [88] obtained large single crystals of the parent PrFeAsO. From pellets of NdFeAsO and LaFeAsO synthesized at high pressure, Martin et al. [71] have been able to isolate crystals with a size up to half a millimeter.

Hence, the 1111 family is currently the least investigated and understood among all FBS, mostly due to the lack of appropriate single crystals. The reported crystals were very tiny and available only for some compositions (**Table 2**), but the research community needs a series of better single crystals to understand the intrinsic properties and to complete the superconducting phase diagram of 1111 without the extrinsic effects. However, the 1111-phase formation and chemical composition are more difficult to control during the growth process. The quality of the crystal can be confirmed by structural and compositional analysis, which are related to superconducting properties. High-pressure techniques (FM-HP), on average, produce sufficiently large crystals when compared to conventional growth methods (FM-AP) [69][77]. Thus, to grow large and homogeneous single crystals, further optimization of the growth conditions is required using the pressure method, including the suitable type of flux.

(b) Solid-State Crystal Growth (SSCG) method: This method utilizes the phenomenon of abnormal grain growth to grow single crystals from a polycrystalline matrix. Recently, Kappenberger et al. [90] reported the growth of large 3-dimensional and facetted single crystals of the parent compound LaFeAsO only using solid-state single crystal growth at ambient pressure (SSCG-AP), as shown in **Figure 4**. This unconventional crystal growth method was successfully used for the first time to grow LaOFeAs crystals with high quality as well as good physical properties. A schematic representation of the SSCG method for growing 1111 single crystals is presented in **Figure 4**a.

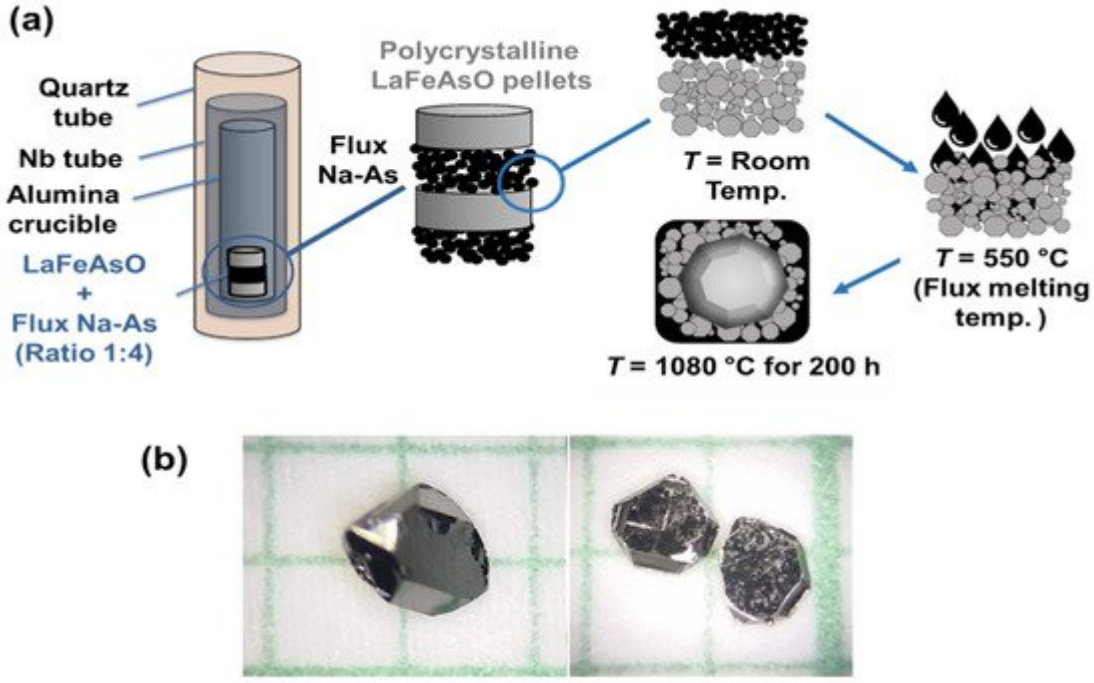

Figure 4. (**a**) A block diagram of the Solid-State Crystal Growth (SSCG) process at ambient pressure (SSCG-AP). The Na-As, as the liquid medium promotor for the growth, is used in between the polycrystalline LaFeAsO pellets.

After annealing, a bimodal size distribution has developed, including large, faceted crystals. (**b**) The grown LaFeAsO single crystals with pronounced facets have a thickness of ~0.4 mm [90].

First, a polycrystalline sample of LaFeAsO was prepared using a two-step solid-state reaction method. Afterward, the polycrystalline powder and Na-As powder in a volume ratio of about 1:1 were layered into an alumina crucible. The Na-As powder melted into a liquid phase at around 550 °C during annealing, diffused into the pores of the polycrystalline compact, and promoted crystal growth. The most important aspect to be mentioned in this report is that NaAs are not a flux, as sometimes misinterpreted in the literature, but only aids in increasing interfacial anisotropy as a trigger for abnormal grain growth [90]. Representative crystals with pronounced facets are shown in **Figure 4**b. These kinds of three-dimensional and faceted crystals are typical for this SSCG method but very uncommon for crystals of the pnictide superconductors and especially for the oxypnictides [90]. This method has been used to grow the crystal for parent compounds, but F-doped 1111 was not successful [90]. Martin et al. [93][71] have grown single crystals of $LaFeAsO_{0.9}F_{0.1}$ and $NdFeAsO_{0.9}F_{0.1}$ using the Solid-State Crystal Growth method at high pressure (SSCG-HP) without the use of a mediator powder (**Table 2**). The crystals were extracted from 5 mm diameter pellets synthesized under high pressure and high temperature, and the value of 10% F substitution is nominally based on the initial stoichiometry of the pellet. More work is needed in this direction with various kinds of doping content.

2. Family 1144

This new family was discovered in November 2016, where some pairs of alkali and alkaline earth elements of varying sizes lead to stoichiometric *AEA*Fe_4As_4 (*AE* = Ca, Sr and *A* = K, Rb, Cs) [54] such as $CaKFe_4As_4$, Sr*A*Fe_4As_4 (*A* = Rb, Cs), $CaRbFe_4As_4$, and $CaCsFe_4As_4$. In essence, their structure is identical to the *AE*Fe_2As_2 structure, just with layer by layer segregation of the *AE* and *A* ions. The reported T_c value for this 1144 family ranges from 31 to 37 K confirmed from magnetic and transport characterizations [54]. Surprisingly, these stoichiometric compounds have such a high T_c without the addition of any doping [54]. Recent studies have established that this family has a very high critical current density (J_c) of the order of 10^8 A/cm^2 and a high H_{c2} (~100 T) with very low anisotropy. Furthermore, J_c has better field dependence than the 122 family and other FBS [94]. Interestingly, high T_c values of the 1144 family are among the highest reported for bulk, fully ordered, stoichiometric FBS [54]. Hence, this family provides a wonderful opportunity to explore the superconducting properties of FBS in a highly ordered compound [102].

Furthermore, extremely high J_c and an isotropic H_{c2} of 1144 indicate significantly improved superconducting properties when compared to other FBS [94][103] families. These experimental findings recommend the 1144 family as a possible strong candidate for superconducting magnet applications where high-quality wires or tapes are required. As we know, wires and tapes for bulk applications are always based on polycrystalline materials, and we need a large quantity of high-quality polycrystalline samples [61]. Hence, an optimization of the synthesis method of 1144 powder is generally required, so that a robust synthesis process can be established for a large amount of the powder sample.

Polycrystalline: Polycrystalline 1144 samples have been synthesized by solid-state reaction (SSR) methods as similar to other FBS, as the general process of SSR is shown in **Figure 1**. For the first time, Iyo et al. [54] synthesized powder $CaKFe_4As_4$ by CSP-AP and found that this new 1144 phase is very sensitive to form two 122 impurity phases of $CaFe_2As_2$ and KFe_2As_2. One should keep in mind that these 122 phases are competitive during the 1144 synthesis process and are more stable than the 1144 phase. In other words, $CaFe_2As_2$ and KFe_2As_2 (122) are the two most common phases that can appear as impurity phases during the formation of $CaKFe_4As_4$. **Table 1** summarizes the reported polycrystalline samples with their superconducting properties. Recently, Singh et al. [102][55] have optimized the pure phase formation of $CaKFe_4As_4$ by preparing the samples in a very broad temperature range using Ta-tube. These samples are characterized by various measurements such as XRD, magnetization, and transport to conclude. These studies find that the synthesis process of the 1144 phase has a very narrow temperature window and a small temperature difference to eliminate the impurity phases. The synthesis conditions of 955 °C for 6 h were the optimum conditions for obtaining pure polycrystalline $CaKFe_4As_4$ with the highest onset T_c value of 34.2 K, a sharp transition width of 2 K, and also a high J_c compared to other 1144 bulk samples [55]. Furthermore, the heating time dependence has also been checked with the best synthesis temperature (955 °C), which showed that samples prepared at 955 °C for a longer period (~17 h) have the tendency to start forming $CaFe_2As_2$ and KFe_2As_2 impurity phases. The field dependence of the calculated J_c for this polycrystal sample at various temperatures shows that the J_c value at 2 K is larger than 10^4 A-cm^{-2} even at 5 T and improved compared with other 1144 polycrystalline samples [55]. However, the order of such a J_c value has also been observed in polycrystalline samples of other FBS families [63][59] and it is larger than that observed in specifically processed C-doped MgB_2 [104][105].

Furthermore, Cheng et al. [106] used the Nb tube for sealing the mixture powder after it was ball milled for 10 h in an Ar atmosphere and heated the sample at 900 °C for 30 h by the CSP-AP. The final product showed some amounts of the impurity phases, such as KFe_2As_2. Recently, Masi et al. [107] carried out the mechanochemical step on precursor powder mixtures before using a solid-state reaction synthesis route (CSP-AP) to produce the $CaKFe_4As_4$ compound. This study suggests that the high-energy ball milling step could act as a promotor for the reaction among the pure elements. This activation process of the powders significantly reduces the synthesis temperature compared to the previous literature (~900 °C). They prepared 1144 samples in the temperature range of 500–700 °C and showed that the 1144 samples prepared at 700 °C had fewer impurity phases than other samples. Masi et al. [107] also reported the effect of an alkaline or alkaline-earth depletion or an iron enrichment on the starting chemical composition: chemical variations are reflected in the formation of secondary phases without, however, significantly influencing the superconducting properties of the samples. The reported critical current density [107] is affected by extrinsic factors presented in the samples, such as pores, impurity phases, and also the observed oxygen contamination at the grain boundaries during the milling process of the powder. These studies indicate that the mechanochemically process plays an important role in reducing the synthesis temperature, which can play a significant role in the development of superconducting wires and tapes in terms of purification and densification processes. Furthermore, Ishida et al. [108] have used the Spark Plasma Sintering (SPS) techniques for the synthesis of $CaKFe_4As_4$ polycrystalline samples and the density of prepared $CaKFe_4As_4$ has been enhanced compared to conventional methods. Interestingly, the prepared 1144 phase is stable up to 500 °C during the post-

annealing process. Above this temperature, the 1144 phase started to degrade into 122 phases ($CaFe_2As_2$ and KFe_2As_2). Even long-time heating such as 17 h at synthesis temperature (955 °C) also degraded the 1144 phase into 122 phases [102][55]. Hence, the reported synthesis phase diagram of 1144 has a very narrow temperature and time window for the preparation of high-quality and large amounts of samples [102][55] by the CSP-AP. A recent study based on the effects of adding low-melting-point metals (Pb, Sn, In, and Ge) to polycrystalline $CaKFe_4As_4$ (CaK1144) superconductors has also been investigated [109]. It showed that Sn addition was effective both to suppress the impurity phases as well as increase the J_c of $CaKFe_4As_4$ without affecting the T_c value, as similar to that reported for Sm1111 [62].

To understand the granular nature of the 1144 family, the remanent magnetization study based on polycrystalline [55] shows the two peaks concerning intergrain and intragrain connectivity as similar to the 1111 family [60][27]. The intergrain J_c of 1144 is shown in **Figure 2**, which is smaller than 122, 1111, and 11 families. This study suggests that the prepared 1144 samples are in a pure phase, but the grain connectivity is very weak due to the presence of many pores inside the sample. This means that, while pure phase formation is important for bulk superconductivity, well-grain connectivity is also required for improved superconducting properties. There is no report based on the HPST.

Single crystal: Since the stoichiometric 1144 phase has four elements, the solution growth method for the single crystal growth is challenging from a four-element melt. Furthermore, the final 1144 phase and its parent 122 phases ($AeFe_2As_2$ and AFe_2As_2) are structurally and chemically similar [54][95]. The first report based on the polycrystalline sample also suggests the similarity of the crystallographic *a*-lattice parameters between 122s is necessary for the formation of the 1144 phase [54]. Hence, during the crystallization process, 1144 phase formations are competed against by these two 122 phases, which could appear as impurities, as discussed above. The list of reported 1144 crystals is summarized in **Table 2** with their growth conditions and superconducting properties. Single crystals of $CaKFe_4As_4$ are grown by high-temperature solution growth from FeAs flux at ambient pressure (FM-AP) [95][103]. As shown in **Figure 3**, the precursor powders were filled up and welded into a Ta-crucible, which was sealed into an evacuated silica ampoule. The growth ampoule was heated to 650 °C for 3 h and then heated to 1180 °C for 5 h. In the next step, it was cooled down to 1050 °C over 2 h, and then slowly cooled from 1050 °C to 930 °C over 30 h [95]. At the end of the reaction, the quartz tube was removed from the furnace to avoid the phase formation of the competent 122 phases. The grown $CaKFe_4As_4$ crystals are mirrorlike plates with a thickness of 100–200 µm which generally depends on the inner diameter of the crucible. Single crystals of $CaKFe_4As_4$ are not particularly air-sensitive and can remain in the air for weeks without any noticeable degradation in their appearance or physical properties [95]. Wang et al. [110] have also grown crystals using the self-flux method (FeAs as a flux) where reaction materials were mixed and ground thoroughly in a mortar with a molar ratio of Ca: K: Fe:As = 1.1: 1: 10: 10. The average size of the grown crystals is ~1 mm. Bao et al. [100] have used RbAs as a flux to grow the millimeter-sized crystals of $RbEuFe_4As_4$ single crystals. These crystals depict the superconducting transition temperature of 36.8 K which is the highest value for the 1144 family. This report also recommends that this flux RbAs can be used to grow the single crystal of other transition metal compounds having the same crystal structure. Furthermore, single crystals of Ni-doped $CaKFe_4As_4$, i.e., $CaK(Fe_{0.949}Ni_{0.051})_4As_4$ were grown from a high-temperature Fe-As rich melt and extensively characterized using thermodynamic and transport

measurements [96]. The selected crystal with dimensions of 4.0 × 4.0 × 0.1 mm^3 was used for the characterizations where the superconducting transition of 9 K and the magnetic ordering transition of ~50 K were observed for $CaK(Fe_{0.949}Ni_{0.051})_4As_4$ crystals [96]. There is not a single report based on the high-pressure growth techniques (FM-HP) [102]. We expect the high-pressure synthesis method for single crystals and polycrystalline samples will further improve the sample quality and its superconducting properties.

References

1. Singh, S.J.; Shimoyama, J.; Yamamoto, A.; Ogino, H.; Kishio, K. Transition Temperature and Upper Critical Field in SmFeAsO1−xFx Synthesized at Low Heating Temperatures. IEEE Trans. Appl. Supercond. 2013, 23, 7300605.
2. Fujioka, M.; Denholme, S.J.; Ozaki, T.; Okazaki, H.; Deguchi, K.; Demura, S.; Hara, H.; Watanabe, T.; Takeya, H.; Yamaguchi, T.; et al. Phase diagram and superconductivity at 58.1 K in α-FeAs-free SmFeAsO1−xFx. Supercond. Sci. Technol. 2013, 26, 085023.
3. Wang, X.-C.; Yu, J.; Ruan, B.B.; Pan, B.J.; Mu, Q.G.; Liu, T.; Zhao, K.; Chen, G.F.; Ren, Z.A. Revisiting the Electron-Doped SmFeAsO: Enhanced Superconductivity up to 58.6 K by Th and F Codoping. Chin. Phys. Lett. 2017, 34, 077401.
4. Kamihara, Y.; Watanabe, T.; Hirano, M.; Hosono, H. Iron-Based Layered Superconductor LaFeAs (x = 0.05−0.12) with Tc = 26 K. J. Am. Chem. Soc. 2008, 130, 3296.
5. Ju, J.; Huynh, K.; Tang, J.; Li, Z.; Watahiki, M.; Sato, K.; Terasaki, H.; Ohtani, E.; Takizawa, H.; Tanigaki, K. Superconducting properties of SmFeAsO1x prepared under high-pressure condition. J. Phys. Chem. Solids 2010, 71, 491.
6. Prakash, J.; Singh, S.J.; Samal, S.L.; Patnaik, S.; Ganguli, A.K. Potassium fluoride doped LaOFeAs multi-band superconductor: Evidence of extremely high upper critical field. Europhys. Lett. 2008, 84, 57003.
7. Prakash, J.; Singh, S.J.; Patnaik, S.; Ganguli, A.K. Upper critical field, superconducting energy gaps and the Seebeck coefficient in La0.8Th0.2FeAsO. J. Phys. Condens. Matter 2009, 21, 175705.
8. Hosono, H.; Yamamoto, A.; Hiramatsu, H.; Ma, Y. Recent advances in iron-based superconductors toward applications. Mater. Today 2018, 21, 278–302.
9. Prakash, J.; Singh, S.J.; Das, D.; Patnaik, S.; Ganguli, A.K. New oxypnictide superconductors: PrOFe1−xCoxAs. J. Solid State Chem. 2010, 183, 338.
10. Prakash, J.; Singh, S.J.; Patnaik, S.; Ganguli, A.K. Superconductivity at 11.3 K induced by cobalt doping in CeFeAsO. Solid State Commun. 2009, 149, 181.

11. Singh, S.J.; Shimoyama, J.; Yamamoto, A.; Ogino, H.; Kishio, K. Effects of Mn and Ni doping on the superconductivity of SmFeAs (O, F). Phys. C Supercond. 2013, 494, 57.
12. Singh, S.J.; Prakash, J.; Pal, A.; Patnaik, S.; Awana, V.P.S.; Ganguli, A.K. Study of Ni and Zn doped CeOFeAs: Effect on the structural transition and specific heat capacity. Phys. C Supercond. 2013, 490, 49.
13. Singh, S.J.; Shimoyama, J.; Yamamoto, A.; Ogino, H.; Kishio, K. Effects of phosphorous doping on the superconducting properties of SmFeAs (O, F). Phys. C Supercond. Its Appl. 2014, 504, 19.
14. Sang, L.N.; Li, Z.; Yang, G.S.; Yue, Z.J.; Liu, J.X.; Cai, C.B.; Wu, T.; Dou, S.X.; Ma, Y.W.; Wang, X.L. Pressure effects on iron-based superconductor families: Superconductivity flux pinning and vortex dynamics. Mater. Today Phys. 2021, 19, 100414.
15. Imai, Y.; Nabeshima, F.; Maeda, A. Comparative Review on Thin Film Growth of Iron-Based Superconductors. Condens. Matter. 2017, 2, 25.
16. Miyazawa, K.; Kihou, K.; Ishikado, M.; Shirage, P.M.; Lee, C.H.; Takeshita, N.; Eisaki, H.; Kito, H.; Iyo, A. Synthesis of LnFeAsO1−y superconductors (Ln= La and Nd) using the high-pressure technique. New J. Phys. 2009, 11, 045002.
17. Mu, G.; Fang, L.; Yang, H.; Zhu, X.; Cheng, P.; Wen, H.H. Doping Dependence of Superconductivity and Lattice Constants in Hole Doped La1-xSrxFeAsO. J. Phys. Soc. Jpn. 2008, 77, 15.
18. Singh, S.J.; Prakash, J.; Patnaik, S.; Ganguli, A.K. Yttrium doped La1−xYxO0.9F0.1FeAs superconductors: Hall and thermopower studies. Phys. C Supercond. 2010, 470, 511.
19. Tropeano, M.; Fanciulli, C.; Canepa, F.; Cimberle, M.R.; Ferdeghini, C.; Lamura, G.; Martinelli, A.; Putti, M.; Vignolo, M.; Palenzona, A. Effect of chemical pressure on spin density wave and superconductivity in undoped and 15% F-doped La1−yYyFeAsO compounds. Phys. Rev. B 2009, 79, 174523.
20. Shirage, P.M.; Miyazawa, K.; Kito, H.; Eisaki, H.; Iyo, A. Superconductivity at 43 K at ambient pressure in the iron-based layered compound La1−xYxFeAsOy. Phys. Rev. B 2008, 78, 172503.
21. Singh, S.J.; Prakash, J.; Patnaik, S.; Gangli, A.K. Enhancement of the superconducting transition temperature and upper critical field of LaO0.8F0.2FeAs with antimony doping. Supercond. Sci. Technol. 2009, 22, 045017.
22. Athena Sefat, S.; Huq, A.; McGuire, M.A.; Jin, R.; Sales, B.C.; Mandrus, D. Superconductivity in LaFe1−xCoxAsO. Phys. Rev. B 2008, 78, 104505.
23. Wang, C.; Jiang, S.; Tao, Q.; Ren, Z.; Li, Y.; Li, L.; Feng, C.; Dai, J.; Cao, G.; Xu, Z. Superconductivity in LaFeAs1−xPxO: Effect of chemical pressures and bond covalency. Europhys. Lett. 2009, 86, 47002.

24. Sato, M.; Kobayashi, Y.; Lee, S.C.; Takahashi, H.; Satomi, E.; Miura, Y. Studies of Impurity-Doping Effects and NMR Measurements of La1111 and/or Nd 1111. J. Phys. Soc. Jpn. 2010, 79, 014710.
25. Miyazawa, K.; Ishida, S.; Kihou, K.; Shirage, P.M.; Nakajima, M.; Lee, C.H.; Kito, H.; Tomioka, Y.; Ito, T.; Eisaki, H.; et al. Possible hydrogen doping and enhancement of Tc in a LaFeAsO based superconductor. Appl. Phys. Lett. 2010, 96, 072514.
26. Prakash, J.; Singh, S.J.; Patnaik, S.; Ganguli, A.K. Superconductivity in CeO1−xFxFeAs with upper critical field of 94 T. Phys. C Supercond. 2009, 469, 82.
27. Prakash, J.; Singh, S.J.; Banerjee, A.; Patnaik, S.; Ganguli, A.K. Enhancement in transition temperature and upper critical field of CeO0.8F0.2FeAs by yttrium doping. Appl. Phys. Lett. 2009, 95, 262507.
28. Luo, Y.; Li, Y.; Jiang, S.; Dai, J.; Cao, G.; Xu, Z. Phase diagram of CeFeAs1−xPxO obtained from electrical resistivity, magnetization, and specific heat measurements. Phys. Rev. B 2010, 81, 134422.
29. Jesche, A.; Forster, T.; Spehling, J.; Nicklas, M.; Souza, M.; Gumeniuk, R.; Luetkens, H.; Goltz, T.; Krellner, C.; Lang, M.; et al. Ferromagnetism and superconductivity in CeFeAs1−xPxO. Phys. Rev. B 2012, 86, 020501.
30. Luo, Y.; Han, H.; Jiang, S.; Lin, X.; Li, Y.; Dai, J.; Cao, G.; Xu, Z. Interplay of superconductivity and Ce 4 f magnetism in CeFeAs1−xPxO0.95F0.05. Phys. Rev. B 2011, 83, 054501.
31. Singh, S.J.; Prakash, J.; Patnaik, S.; Ganguli, A.K. Effects of simultaneous carrier doping in the charge reservoir and conducting layers of superconducting CeO0.9F0.1Fe1−xCoxAs. Phys. C Supercond. 2010, 470, 1928.
32. Prakash, J.; Singh, S.J.; Thakur, G.; Patnaik, S.; Ganguli, A.K. The effect of antimony doping on the transport and magnetic properties of Ce(O/F)FeAs. Supercond. Sci. Technol. 2011, 24, 125008.
33. Bhoi, D.; Mandal, P.; Choudhury, P. Normal-state transport properties of PrFeAsO1−xFy superconductor. Phys. C Supercond. 2008, 468, 2275.
34. Lin, X.; Guo, H.; Shen, C.; Tao, Q.; Cao, G.; Xu, Z. Superconductivity in Sr and Co co-doped PrFeAsO. J. Phys. Chem. Solids 2011, 72, 434.
35. Kito, H.; Eisaki, H.; Iyo, A. Superconductivity at 54 K in F-Free NdFeAsO1-y. J. Phys. Soc. Jpn. 2008, 77, 063707.
36. Kursumovic, A.; Durrell, J.H.; Chen, S.K.; MacManus-Driscoll, J.L. Ambient/low pressure synthesis and fast densification to achieve 55 K Tc superconductivity in NdFeAsO0.75F0.25. Supercond. Sci. Technol. 2009, 23, 025022.

37. Lamura, G.; Shiroka, T.; Bonfà, P.; Sanna, S.; Renzi, R.D.; Putti, M.; Zhigadlo, N.D.; Katrych, S.; Khasanov, R.; Karpinski, J. Slow magnetic fluctuations and superconductivity in fluorine-doped NdFeAsO. Phys. Rev. B 2015, 91, 024513.
38. Aswathy, P.M.; Anooja, J.B.; Varghese, N.; Syamaprasad, U.U. Enhanced transport and magnetic properties in gadolinium doped NdFeAsO0.7F0.3 superconductors. AIP Conf. Proc. 2015, 1665, 130047.
39. Bérardan, D.; Zhao, L.; Pinsard-Gaudart, L.; Dragoe, N. Electronic phase diagram of NdFe1−xRhxAsO. Phys. Rev. B 2010, 81, 094506.
40. Lee, S.C.; Satomi, E.; Kobayashi, Y.; Sato, M. Effects of Ru Doping on the Transport Behavior and Superconducting Transition Temperature of NdFeAsO0.89F0.11. J. Phys. Soc. Jpn. 2010, 79, 023702.
41. Tehrani, F.S.; Daadmehr, V. Superconductivity Versus Structural Parameters in Calcium-Doped Nd1-xCaxFeAsO0.8F0.2 Superconductors. J. Supercond. Nov. Magn. 2020, 33, 337.
42. Marcinkova, A.; Grist, D.A.M.; Margiolaki, I.; Hansen, T.C.; Margadonna, S.; Bos, J.W. Superconductivity in NdFe1-xCoxAsO. Phys. Rev. B 2010, 81, 064511.
43. Qi, Y.; Gao, Z.; Wang, L.; Wang, D.; Zhang, X.; Ma, Y. Superconductivity in Co-doped SmFeAsO. Supercond. Sci. Technol. 2008, 21, 115016.
44. Chen, H.; Zheng, M.; Fang, A.; Yang, J.; Huang, F.; Xie, X.; Jiang, M. Enhanced superconductivity of SmFeAsO co-doped by Scandium andFluorine to increase chemical inner pressure. J. Solid State Chem. 2012, 194, 59.
45. Lai, K.T.; Kwong, F.L.; Ng, D.H.L. Superconductivity in fluorine and yttrium co-doped SmFeAsO. J. Appl. Phys. 2012, 111, 093912.
46. Chen, Y.L.; Cheng, C.H.; Cui, Y.J.; Zhang, H.; Zhang, Y.; Yang, Y.; Zhao, Y. Ir Doping-Induced Superconductivity in the SmFeAsO System. J. Am. Chem. Soc. 2009, 131, 10338–10339.
47. Wang, C.; Li, L.; Chi, S.; Zhu, Z.; Ren, Z.; Li, Y.; Wang, Y.; Lin, X.; Luo, Y.; Jiang, S.; et al. Thorium-doping–induced superconductivity up to 56 K in Gd1−xThxFeAsO. Europhys. Lett. 2008, 83, 67006.
48. Yang, J.; Li, Z.C.; Lu, W.; Yi, W.; Shen, X.L.; Ren, Z.A.; Che, G.C.; Dong, X.L.; Sun, L.L.; Zhou, F.; et al. Superconductivity at 53.5 K in GdFeAsO1−δ. Supercond. Sci. Technol. 2008, 21, 082001.
49. Zhou, Y.; Sidorov, V.A.; Petrova, A.E.; Penkov, A.A.; Pinyagin, A.N.; Zhao, Z.; Sun, L. Superconducting Properties of GdFeAsO0.85 at High Pressure. J. Supercond. Mag. 2016, 29, 1105.
50. Cheng, P.; Fang, L.; Yang, H.; Zhu, X.Y.; Mu, G.; Luo, H.Q.; Wang, Z.S.; Wen, H.H. Superconductivity at 36 K in gadolinium-arsenide oxides GdO1−xFxFeAs. Sci. China Ser. G

Phys. Mech. Astron. 2008, 51, 719.

51. Cui, Y.; Chen, Y.L.; Cheng, C.H.; Yang, Y.; Jiang, J.; Wang, Y.Z.; Zhang, Y.; Zhao, Y. Superconductivity and magnetism in Ir-doped GdFeAsO. Phys. C Supercond. Its Appl. 2010, 470, 1077.
52. Wu, G.; Xie, Y.L.; Chen, H.; Zhong, M.; Liu, R.H.; Shi, B.C.; Li, Q.J.; Wang, X.F.; Wu, T.; Yan, Y.J. Superconductivity at 56 K in Samarium-doped SrFeAsF. J. Phys.: Condens. Matter. 2009, 21, 142203.
53. Matsuishi, S.; Inoue, Y.; Nomura, T.; Yanagi, H.; Hirano, M.; Hosono, H. Superconductivity Induced by Co-Doping in Quaternary Fluoroarsenide CaFeAsF. J. Am. Chem. Soc. 2008, 130, 14428–14429.
54. Iyo, A.; Kawashima, K.; Kinjo, T.; Nishio, T.; Ishida, S.; Fujihisa, H.; Gotoh, Y.; Kihou, K.; Eisaki, H.; Yoshida, Y. New-Structure-Type Fe-Based Superconductors: CaAFe4As4 (A = K, Rb, Cs) and SrAFe4As4 (A = Rb, Cs). J. Am. Chem. Soc. 2016, 138, 3410–3415.
55. Singh, S.J.; Cassidy, S.J.; Bristow, M.; Blundell, S.J.; Clarke, S.J.; Coldea, A.I. Optimization of superconducting properties of the stoichiometric CaKFe4As4. Supercond. Sci. Technol. 2020, 33, 025003.
56. Fujioka, M.; Denholme, S.J.; Tanaka, M.; Takeya, H.; Yamaguchi, T.; Takano, Y. The effect of exceptionally high fluorine doping on the anisotropy of single crystalline SmFeAsO1−xFx. Appl. Phys. Lett. 2014, 105, 102602.
57. Malavasi, L.; Artioli, G.A.; Ritter, C.; Mozzati, M.C.; Maroni, B.; Pahari, B.; Caneschi, A. Phase Diagram of NdFeAsO1−xFx: Essential Role of Chemical Composition. J. Am. Chem. Soc. 2010, 132, 2417.
58. Kametani, F.; Polyanskii, A.A.; Yamamoto, A.; Jiang, J.; Hellstrom, E.E.; Gurevich, A.; Larbalestier, D.C.; Ren, Z.A.; Yang, J.; Dong, X.L.; et al. Combined microstructural and magneto-optical study of current flow in polycrystalline forms of Nd and Sm Fe-oxypnictides. Supercond. Sci. Technol. 2008, 22, 015010.
59. Yamamoto, A.; Jiang, J.; Kametani, F.; Polyanskii, A.; Hellstrom, E.; Larbalestier, D.; Martinelli, A.; Palenzona, A.; Tropeano, M.; Putti, M. Evidence for electromagnetic granularity in polycrystalline Sm1111 iron-pnictides with enhanced phase purity. Supercond. Sci. Technol. 2011, 24, 045010.
60. Singh, S.J.; Shimoyama, J.; Yamamoto, A.; Ogino, H.; Kishio, K. Significant enhancement of the intergrain coupling in lightly F-doped SmFeAsO superconductors. Supercond. Sci. Technol. 2013, 26, 065006.
61. Yao, C.; Ma, Y. Recent breakthrough development in iron-based superconducting wires for practical applications. Supercond. Sci. Technol. 2019, 32, 023002.

62. Singh, S.J.; Shimoyama, J.; Ogino, H.; Yamamoto, A.; Kishio, K. Enhancement of intergranular current density of Sm-based oxypnictide superconductors with Sn addition. Supercond. Sci. Technol. 2014, 27, 085010.
63. Singh, S.J.; Robert, B.; Wurmehl, S.; Hess, C.; Buechner, B. Granular behavior observed in the polycrystalline superconducting LiFeAs. Supercond. Sci. Technol. 2015, 28, 025006.
64. Singh, S.J.; Ogino, H.; Shimoyama, J.; Kishio, K. Weak-link behaviour observed in iron-based superconductors with thick perovskite-type blocking layers. Supercond. Sci. Technol. 2013, 26, 105020.
65. Otabe, E.S.; Kiuchi, M.; Kawai, S.; Morita, Y.; Ge, J.; Ni, B.; Gao, Z.; Wang, L.; Qi, Y.; Zhang, X.; et al. Global and local critical current density in superconducting SmFeAsO1−xFx measured by two methods. Phys. C Supercond. 2009, 469, 1940.
66. Hayashi, Y.; Yamamoto, A.; Ogino, H.; Shimoyama, J.; Kishio, K. Influences of material processing on the microstructure and inter-granular current properties of polycrystalline bulk Ba(Fe,Co)2As2. Physica C Supercond. Its Appl. 2014, 504, 28.
67. Yoshida, N.; Kiuchi, M.; Otabe, E.S.; Matsushita, T.; Ge, J.; Ni, B.; Wang, L.; Qi, Y.; Zhang, X.; Gao, Z.; et al. Critical current density properties in polycrystalline Sr0.6K0.4Fe2As2 superconductors. Phys. C Supercond. Its Appl. 2010, 470, 1216.
68. Palenzona, A.; Sala, A.; Bernini, C.; Braccini, V.; Cimberle, M.R.; Ferdeghini, C.; Lamura, G.; Martinelli, A.; Pallecchi, I.; Romano, G.; et al. A new approach for improving global critical current density in Fe(Se0.5Te0.5) polycrystalline materials. Supercond. Sci. Technol. 2012, 25, 115018.
69. Karpinski, J.; Zhigadlo, N.D.; Katrych, S.; Bukowski, Z.; Moll, P.; Weyeneth, S.; Keller, H.; Puzniak, R.; Tortello, M.; Daghero, D.; et al. Single crystals of LnFeAsO1-xFx (Ln = La, Pr, Nd, Sm, Gd) and Ba1-xRbxFe2As2. Physica C 2009, 469, 370.
70. Quebe, P.; Terbüchte, L.J.; Jeitschko, W. Quaternary rare earth transition metal arsenide oxides RTAsO (T = Fe, Ru, Co) with ZrCuSiAs type structure. J. Allyos Cmpds. 2000, 302, 70.
71. Martin, C.; Tillman, M.E.; Kim, H.; Tanatar, M.A.; Kim, S.K.; Kreyssig, A.; Gordon, R.T.; Vannette, M.D.; Nandi, S.; Kogan, V.G.; et al. Nonexponential London Penetration Depth of FeAs-Based Superconducting ReFeAsO0.9F0.1 (R = La, Nd) Single Crystals. Phys. Rev. Lett. 2009, 102, 247002.
72. Fang, L.; Cheng, P.; Jia, Y.; Zhu, X.; Luo, H.; Mu, G.; Gu, C.; Wen, H.H. Growthof NdFeAs(O,F) single crystals at ambient pressure and their properties. J. Cryst. Growth 2009, 311, 358.
73. Jesche, A.; Krellner, C.; Souza, M.; Lang, M.; Geibel, C. Rare earth magnetism in CeFeAsO: A single crystal study. New J. Phys. 2009, 11, 103050.

74. Nitsche, F.; Jesche, A.; Hieckmann, E.; Doert, T.H.; Ruck, M. Structural trends from a consistent set of single-crystal data of RFeAsO (R = La, Ce, Pr, Nd, Sm, Gd, and Tb). Phys. Rev. B 2010, 82, 134514.
75. Rutzinger, D.; Bartsch, C.; Doerr, M.; Rosner, H.; Neu, V.; Doert, T.; Ruck, M. Lattice distortions in layered type arsenides LnTAs2 (Ln = La–Nd, Sm, Gd, Tb; T = Ag, Au): Crystal structures, electronic and magnetic properties. J. Solid State Chem. 2010, 183, 510.
76. Hanna, A.R.N.; Abdel-Hafiez, M. Single-Crystal Growth and Small Anisotropy of the Lower Critical Field in Oxypnictides: NdFeAsO1-xFx. Crystals 2020, 10, 362.
77. Zhigadlo, N.D.; Weyeneth, S.; Katrych, S.; Moll, P.J.W.; Rogacki, K.; Bosma, S.; Puzniak, R.; Karpinski, J.; Batlogg, B. High-pressure flux growth, structural, and superconducting properties of LnFeAsO. Phys. Rev. B 2012, 86, 214509.
78. Sefat, A.S.; Jin, R.; McGuire, M.A.; Sales, B.C.; Singh, D.J.; Mandrus, D. Superconductivity at 22 K in Co-Doped BaFe2As2 Crystals. Phys. Rev. Lett. 2008, 101, 117004.
79. Rotter, M.; Tegel, M.; Johrendt, D. Superconductivity at 38 K in the Iron Arsenide (Ba1−xKx)Fe2As2. Phys. Rev. Lett. 2008, 101, 107006.
80. Ishida, S.; Song, D.; Ogino, H.; Iyo, A.; Eisaki, H.; Nakajima, M.; Shimoyama, J.; Eisterer, M. Doping-dependent critical current properties in K, Co, and P-doped BaFe2As2 single crystals. Phys. Rev. B 2017, 95, 014517.
81. Demirdis, S.; Fasano, Y.; Kasahara, S.; Terashima, T.; Shibauchi, T.; Matsuda, Y.; Konczykowski, M.; Pastoriza, H.; Beek, C.J. Disorder, critical currents, and vortex pinning energies in isovalently substituted BaFe2(As1-xPx)2. Phys. Rev. B 2013, 87, 094506.
82. Shen, B.; Cheng, P.; Wang, Z.; Fang, L.; Ren, C.; Shan, L.; Wen, H.H. Flux dynamics and vortex phase diagram in Ba(Fe,Co)2As2 single crystals revealed by magnetization and its relaxation. Phys. Rev. B 2010, 81, 014503.
83. Song, D.; Ishida, S.; Iyo, A.; Nakajima, M.; Shimoyama, J.; Eisterer, M.; Eisaki, H. Distinct doping dependence of critical temperature and critical current density in Ba1−xKxFe2As2 superconductor. Sci. Rep. 2016, 6, 26671.
84. Prozorov, R.; Tanatar, M.A.; Ni, N.; Kreyssig, A.; Nandi, S.; Bud'ko, S.L.; Goldman, A.I.; Canfield, P.C. Intrinsic pinning on structural domains in underdoped single crystals of Ba(Fe,Co)2As2. Phys. Rev. B 2009, 80, 174517.
85. Yan, J.Q.; Nandi, S.; Zarestky, J.L.; Tian, W.; Kreyssig, A.; Jensen, B.; Kracher, A.; Dennis, K.W.; McQueeney, R.J.; Goldman, A.I.; et al. Flux growth at ambient pressure of millimeter-sized single crystals of LaFeAsO, LaFeAsO1−xFx, and LaFe1−xCoxAsO. Appl. Phys. Lett. 2009, 95, 222504.

86. Iimura, S.; Muramoto, T.; Fujitsu, S.; Matsuishi, S.; Hosono, H. High pressure growth and electron transport properties of superconducting SmFeAsO1−xHx single crystals. J. Asian Ceram. Soc. 2017, 5, 357.

87. Yan, J.-Q.; Jensen, B.; Dennis, K.W.; McCallum, R.W.; Lograsso, T.A. Flux requirements for the growth of RFeAsO (R = rare earth) superconductors. Appl. Phys. Lett. 2011, 98, 072504.

88. Ishikado, M.; Shamoto, S.; Kito, H.; Iyo, A.; Eisaki, H.; Ito, T.; Tomioka, Y. Growth of single crystal PrFeAsO1-y and its characterization. Physica C 2009, 469, 901.

89. Yan, J.Q.; Xing, Q.; Jensen, B.; Xu, H.; Dennis, K.W.; McCallum, R.W.; Lograsso, T.A. Contamination from magnetic starting materials in flux-grown single crystals of RFeAsO superconductors. Phys. Rev. B 2011, 84, 012501.

90. Kappenberger, R.; Aswartham, S.; Scaravaggi, F.; Blum, C.; Sturza, M.I.; Wolter, A.U.B.; Wurmehl, S.; Büchner, B. Solid state single crystal growth of three-dimensional faceted LaFeAsO crystals. J. Cryst. Growth 2018, 483, 9.

91. Ma, Y.; Hu, K.; Ji, Q.; Gao, B.; Zhang, H.; Mu, G.; Huang, F.; Xie, X. Growth and characterization of CaFe1-xCoxAsF single crystals by CaAs flux method. J. Cryst. Growth 2016, 451, 161–164.

92. Holder, M.G.; Jesche, A.; Lombardo, P.; Hayn, R.; Vyalikh, D.V.; Kummer, K.; Danzenbächer, S.; Krellner, C.; Geibel, C.; Rienks, E.D.L.; et al. How chemical pressure affects the fundamental properties of rare-earth pnictides: An ARPES view. Phys. Rev. B 2012, 86, 020506.

93. Prozorov, R.; Tillman, M.E.; Mun, E.D.; Canfield, P.C. Intrinsic magnetic properties of the superconductor NdFeAsO0.9F0.1 from local and global measurements. New J. Phys. 2009, 11, 035004.

94. Singh, S.J.; Bristow, M.; Meier, W.R.; Taylor, P.; Blundell, S.J.; Canfield, P.C.; Coldea, A.I. Ultrahigh critical current densities, the vortex phase diagram, and the effect of granularity of the stoichiometric high-Tc superconductor CaKFe4As4. Phys. Rev. Mater. 2018, 2, 074802.

95. Meier, W.R.; Kong, T.; Bud'ko, S.L.; Canfield, P.C. Optimization of the crystal growth of the superconductor CaKFe4As4 from solution in the FeAs-CaFe2As2-KFe2As2 system. Phys. Rev. Mater. 2017, 1, 013401.

96. Meier, R.W.; Ding, Q.P.; Kreyssig, A.; Bud'ko, S.L.; Sapkota, A.; Kothapalli, K.; Borisov, V.; Valentí, R.; Batista, C.D.; Orth, P.P.; et al. Hedgehog spin-vortex crystal stabilized in a hole-doped iron-based superconductor. NPJ Quantum Mater. 2018, 3, 5.

97. Stillwell, R.L.; Wang, X.; Wang, L.; Campbell, D.J.; Paglione, J.; Weir, S.T.; Vohra, Y.K.; Jeffries, J.R. Observation of two collapsed phases in CaRbFe4As4. Phys. Rev. B 2019, 100, 045152.

98. Vlasenko, V.; Pervakov, K.; Gavrilkin, S. Vortex pinning and magnetic phase diagram of EuRbFe4As4 iron-based superconductor. Supercond. Sci. Technol. 2020, 33, 084009.

99. Collomb, D.; Bending, S.J.; Koshelev, A.E.; Smylie, M.P.; Farrar, L.; Bao, J.K.; Chung, D.Y.; Kanatzidis, M.G.; Kwok, W.K.; Welp, U. Observing the Suppression of Superconductivity in RbEuFe4As4 by Correlated Magnetic Fluctuations. Phys. Rev. Lett. 2021, 126, 157001.
100. Bao, J.K.; Willa, K.; Smylie, M.P.; Chen, H.; Welp, U.; Chung, D.Y.; Kanatzidis, M.G. Single Crystal Growth and Study of the Ferromagnetic Superconductor RbEuFe4As4. Cryst. Growth Des. 2018, 18, 3517.
101. Yan, J.-Q. Flux growth utilizing the reaction between flux and crucible. J. Cryst. Growth 2015, 416, 62.
102. Singh, S.J.; Morawski, A. New Potential Family of Iron Based Superconductors towards practical application: CaKFe4As4. In High-Tc Superconducting Technology: Towards Sustainable Development Goals; Jenny Stanford Publishing: New York, NY, USA, 2021; pp. 283–314.
103. Meier, W.R.; Kong, T.; Kaluarachchi, U.S.; Taufour, V.; Jo, N.H.; Drachuck, G.; Böhmer, A.E.; Saunders, S.M.; Sapkota, A.; Kreyssig, A.; et al. Anisotropic thermodynamic and transport properties of single-crystalline CaKFe4As4. Phys. Rev. B 2016, 94, 064501.
104. Buzea, C.; Yamashita, T. Review of the superconducting properties of MgB2. Supercond. Sci. Technol. 2001, 14, R115.
105. Eisterer, M. Magnetic properties and critical currents of MgB2. Supercond. Sci. Technol. 2007, 20, R47–R73.
106. Cheng, Z.; Liu, S.; Dong, C.; Huang, H.; Li, L.; Zhu, Y.; Awaji, S.; Ma, Y. Effects of core density and impurities on the critical current density of CaKFe4As4 superconducting tapes. Supercond. Sci. Technol. 2019, 32, 105014.
107. Masi, A.; Armenio, A.A.; Celentano, G.; Barbera, A.L.; Rufoloni, A.; Silva, E.; Vannozzi, A.; Varsano, F. The role of chemical composition in the synthesis of Ca/K-1144 iron based superconductors. J. Alloys Compd. 2021, 869, 159202.
108. Ishida, S.; Naik, S.P.; Tsuchiya, Y.; Mawatari, Y.; Yoshida, Y.; Iyo, A.; Eisaki, H.; Kamiya, Y.; Kawashima, K.; Ogino, H. Synthesis of CaKFe4As4 bulk samples with high critical current density using a spark plasma sintering technique. Supercond. Sci. Technol. 2020, 33, 094005.
109. Naik, S.; Ishida, S.; Kamiya, Y.; Tsuchiya, Y.; Kawashima, K.; Eisaki, H.; Iyo, A.; Ogino, H. Sn addition effects on CaKFe4As4 superconductors. Supercond. Sci. Technol. 2020, 33, 104004.
110. Wang, C.; He, T.; Han, Q.; Fan, C.; Tang, Q.; Chen, D.; Lei, Q.; Sun, S.; Li, Y.; Yu, B. Novel sample-thickness-dependent flux pinning behaviors of KFe2As2 intercalations in CaKFe4As4 single crystals. Supercond. Sci. Technol. 2021, 34, 055001.